





# Approximation Methods for Simulation and Equivalence Checking of Noisy Quantum Circuits

Mingyu Huang , Ji Guan , Wang Fang , and Mingsheng Ying 

**Abstract**—In the current NISQ (Noisy Intermediate-Scale Quantum) era, simulating and verifying noisy quantum circuits is crucial but faces challenges such as quantum state explosion and complex noise representations, constraining simulation, and equivalence checking to circuits with a limited number of qubits. This paper introduces an approximation algorithm for simulating and assessing the equivalence of noisy quantum circuits, specifically designed to improve scalability under low-noise conditions. The approach utilizes a novel tensor network diagram combined with singular value decomposition to approximate the tensors of quantum noises. The implementation is based on Google’s TensorNetwork Python package for contraction. Experimental results on realistic quantum circuits with realistic hardware noise models indicate that our algorithm can simulate and check the equivalence of QAOA (Quantum Approximate Optimization Algorithm) circuits with around 200 qubits, surpassing the state-of-the-art methods by noise number and execution time.

**Index Terms**—Quantum circuits, noisy simulation, equivalence checking, approximation algorithm, tensor network

## I. INTRODUCTION

SINCE achieving quantum supremacy over classical computing [1], quantum processors with an increasing number of qubits have been manufactured, marking a significant milestone in the development of quantum computing. These advancements in quantum hardware have opened up new possibilities for computation, pushing the boundaries of what is possible with traditional classical computers. Notable examples of quantum processors with expanding qubit counts include those developed by leading organizations such as Google [2] and IBM [3]. These processors are poised to handle more complex and larger-scale computations, a critical step towards achieving broader and more practical applications in quantum computing. This progress has marked the transition into what is commonly referred to as the NISQ (Noisy Intermediate-Scale Quantum) era [4], a phase in quantum computing where devices have an intermediate number of qubits, typically ranging from a few tens to a few hundred, but are still prone to various types of noise and error. Despite these limitations, NISQ devices hold considerable promise for specific tasks that could not be efficiently solved with classical computing, even if they do not yet reach the fault tolerance

required for large-scale, error-corrected quantum computers. The challenges of noise, decoherence, and limited qubit counts in current quantum processors have prompted researchers to develop new algorithms and methods, such as quantum error correction [5, 6, 7] and error mitigation strategies [8, 9, 10], that aim to improve the performance of NISQ devices.

Even though current quantum processors have a limited number of qubits and are susceptible to quantum noise, they have already been used in a variety of applications, demonstrating their potential benefits in fields like optimization, chemistry, material science, and machine learning [11, 12, 13]. At the core of these quantum systems lies the quantum circuit, which represents the essential framework for quantum computation. The design and execution of quantum circuits enable quantum computers to perform calculations that would otherwise be impossible with classical systems. As quantum hardware advances, optimizing the structure, execution, and error resilience of quantum circuits will be crucial to unlocking the full potential of quantum computing. In this context, simulating and performing equivalence checking of quantum circuits have become vital steps for ensuring the correctness and efficiency of quantum computations.

### A. Noisy Simulation

In classical computation, the complexity of testing and verifying digital circuits has necessitated the development of a comprehensive tool chain designed to assist engineers in the rigorous process of ensuring circuit reliability and functionality. Central to this workflow is fault simulation, a critical technique used to model and analyze potential errors in circuit operations. Fault simulation plays a pivotal role in identifying and understanding how various fault models, such as stuck-at faults or bridging faults, can affect the behavior of a circuit. The workflow typically begins with generating a set of specific inputs (test patterns) to detect these faults. These patterns are then applied to a fault simulator, which assesses the circuit’s response to each possible fault [14]. The results from fault simulation inform the subsequent stages of the workflow, including design for testability (DFT) strategies and automatic test pattern generation (ATPG) as illustrated in Fig. 1.

In the quantum era, the methodology for testing and verifying circuits is fundamentally redefined, adapting to the unique properties of quantum systems. This difference is driven by the intrinsic differences between classical digital circuits and their quantum counterparts.

- **Test Circuit:** Central to quantum circuits are unitary gates manipulating quantum bits (qubits), unlike the logical

Mingyu Huang and Ji Guan are with Key Laboratory of System Software (Chinese Academy of Sciences) and State Key Laboratory of Computer Science, Institute of Software, Chinese Academy of Sciences, Beijing 101408, China (e-mail: huangmy@ios.ac.cn; guanji@ios.ac.cn).

Wang Fang is with the School of Informatics, University of Edinburgh, Edinburgh EH8 9UR, United Kingdom (email: wang.fang@ed.ac.uk).

Mingsheng Ying is with Centre for Quantum Software and Information, University of Technology Sydney, Ultimo NSW 2007, Australia (e-mail: Mingsheng.Ying@uts.edu.au).

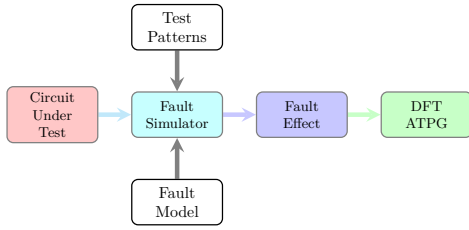


Fig. 1: Test Workflow of Classical Circuit.

gates acting on classical bits. A significant challenge in simulation of quantum computing on classical computers is the representation of quantum states. Unlike classical states, which are represented by bit strings, quantum states require an exponential space. This exponential scaling complicates the analysis of quantum circuits.

- **Noise (Fault) Model:** In the current NISQ (Noisy Intermediate-Scale Quantum) era, real-world quantum circuits are notably affected by various noises analogous to faults in classical circuits. The nature of noise in quantum circuits vastly differs from classical fault models due to the diverse physical implementations of quantum computing, such as superconducting and ion-trapping methods. Each method introduces unique noise characteristics; for example, decoherence is a significant issue in superconducting quantum circuits. Addressing these noise factors requires a specialized approach to model and mitigate faults in quantum systems.

These differences fundamentally distinguish simulating a noisy quantum circuit from its classical counterpart. Therefore, efficient simulation algorithms for noisy quantum circuits need to be developed urgently.

### B. (Approximate) Equivalence Checking

Equivalence checking plays a pivotal role in electronic design automation (EDA), particularly in verifying the correctness of circuits during the design process. This method is essential in ensuring that a circuit performs its intended function accurately after undergoing various design and optimization stages. By comparing the behavior of a circuit at different levels of abstraction, such as between a high-level functional specification and a lower-level implementation (like Register Transfer Level, or RTL), equivalence checking guarantees that any modifications, enhancements, or optimizations do not inadvertently alter the circuit's fundamental operation. This verification process is indispensable in the development of reliable and efficient electronic systems, as it helps to identify and rectify errors early in the design phase, thereby saving time, reducing costs, and ensuring the final product meets quality and performance standards [14].

Unlike classical circuits, which are characterized by different levels of abstraction, current quantum circuits do not yet have such distinct layers. Nevertheless, the presence of noise in realistic quantum circuits necessitates the evaluation of their performance under specific noise models. Understanding the impact of noise is crucial to determine if a quantum circuit

can function as intended. It is particularly valuable to predict the extent to which a real-world quantum circuit, affected by noise, can align with the performance of its ideal, noise-free counterpart. This assessment is key to advancing quantum computing, as it helps design more robust quantum circuits capable of withstanding the practical challenges posed by environmental interference and system imperfections.

### C. Contributions of This Paper

Despite significant advancements in the *design automation research* for quantum computing, challenges like the quantum state explosion problem persist. Current simulation and equivalence checking capabilities are limited to real application circuits with tens of qubits. This limitation poses significant issues for Noisy Intermediate-Scale Quantum (NISQ) circuits, which often consist of hundreds of qubits and require efficient simulation and verification tools. To bridge this gap, we propose a novel approximation algorithm for simulating and performing equivalence checks on noisy quantum circuits.

Our key contribution is introducing an approximation algorithm framework based on a tensor network diagram tailored to these tasks. In this framework, noisy quantum circuits are represented as double-size tensor networks, and noise operators are effectively approximated through Singular Value Decomposition (SVD) applied to their tensor representations. Leveraging this decomposition, we develop approximation algorithms for simulation and equivalence checking of noisy quantum circuits and implement it using Google's *TensorNetwork* [15] package.

The efficacy and practicality of our algorithm are demonstrated through extensive experiments on five distinct types of quantum circuits (algorithms). Our results indicate that the proposed method can approximately simulate and verify the equivalence of real application circuits with up to 200 qubits and 20 noise operations. Notably, our approach outperforms state-of-the-art approximation techniques, including the quantum trajectories method [16] and the Matrix Product Operators (MPO)-based simulation method, regarding computational efficiency and scalability.

### D. Organization of the Paper:

In Section II we introduce the basics of quantum computation. In Section III, we give the formal definition of the noisy simulation task and show a tensor network diagram as the basis of our approximate algorithm. The description of our approximate noisy simulation method and the analysis of its precision are presented in Section IV. In Section V, we develop an approximate equivalence checking algorithm based on the approximation techniques introduced in Section IV. Finally, we evaluate the runtime and precision of our algorithms in Section VI.

### E. Related Works

1) *Simulation of Quantum Circuits:* Simulating quantum circuits is a core task in design automation for quantum computing, particularly for noiseless circuits. The standard

approach for simulation involves state vector evolution through matrix multiplication, which is widely implemented in frameworks such as Qiskit and Cirq. However, the exponential growth of state vectors with increasing qubits severely limits the scalability of this approach. To overcome this challenge, tensor network methods leverage the locality (gates operate on a limited number of qubits) and regularity (structured gate patterns) inherent in quantum circuits. These methods enable efficient simulation of large noiseless circuits [17, 18, 19, 20, 21, 22]. Decision Diagram (DD)-based methods, inspired by classical Binary Decision Diagrams (BDDs), further optimize memory and performance by compactly representing state amplitudes [23, 24]. However, DD-based methods struggle to handle circuits with arbitrary parameterized gates, such as those found in quantum supremacy experiments [23, 25].

Furthermore, for noisy quantum circuits, density matrix representations are commonly employed. However, their scalability is severely limited by the exponential growth of the Hilbert space with the number of qubits. To mitigate this, approximation techniques such as the quantum trajectories method [16, 26] have been developed. The quantum trajectories method is a Monte Carlo-based approach for simulating noisy quantum circuits. It works by probabilistically sampling the Kraus operators associated with noise channels and averaging the results obtained from multiple samples. By decomposing noise operators into Kraus matrices, the simulation of each sample reduces to a noiseless quantum circuit simulation task. This allows the method to leverage various noiseless simulation backends. For instance, Google’s quantum trajectory-based noisy circuit simulator, `qsim` [16], employs matrix-vector multiplication as its computational backend. Similarly, a decision diagram (DD)-based backend for quantum trajectories has been implemented in `DDSIM` [26]. Tensor network-based methods, such as Matrix Product States (MPS), Matrix Product Operators (MPO), and Matrix Product Density Operators (MPDO), offer another avenue for efficient simulation. These techniques rely on Singular Value Decomposition (SVD) to compress and manipulate quantum states and operators, enabling scalable simulations for certain classes of circuits [27, 28, 29, 30].

Despite these advancements, simulating large, complex circuits with significant noise remains challenging. To address these issues, we propose an approximation algorithm based on tensor network diagrams. Our approach achieves greater computational efficiency, especially at low noise levels, compared to the quantum trajectories method and MPO-based techniques.

2) *Equivalence Checking of Quantum Circuits*: Equivalence checking of combinational quantum circuits has been extensively studied, with methods based on Quantum Multiple Decision Diagrams (QMDDs) [31, 32, 33]. Additionally, Tensor Decision Diagrams (TDD) have been developed to check the equivalence of both combinational and dynamic quantum circuits [34, 35], where the latter use measurement outputs to control other parts of the circuit. Most equivalence checking techniques focus on determining the exact equality between two circuits (up to a global phase). In contrast, we focus on approximate equivalence, as proposed in [34]. Our approach

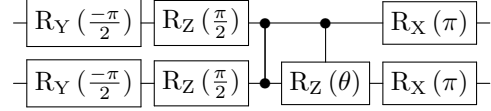


Fig. 2: A 2-qubit QAOA circuit

provides a more efficient algorithm for checking the equivalence of noisy quantum circuits, improving performance in practical applications where exact equivalence is not feasible.

3) *Relation to Our Previous Work*: A preliminary version of our approximation simulation method was presented as a conference paper [36]. This paper significantly extends that research by applying the method to the equivalence checking task and enhancing existing approximation and equivalence checking techniques. Through additional experiments and analysis, we demonstrate the effectiveness of our approach, providing further evidence of its applicability.

## II. PRELIMINARY

**Basics of Quantum Computation:** We start by recalling some basic concepts of quantum circuits. Ideally, a quantum computer without noise is a closed system. In this case, quantum data are mathematically modeled as complex unit vectors in a  $2^n$ -dimensional Hilbert (linear) space  $\mathcal{H}$ . Such a quantum datum is usually called a *pure state* and written as  $|\psi\rangle$  in the Dirac notation, and  $n$  represents the number of involved *quantum bits (qubits)*. Specifically, a qubit is a quantum datum in a 2-dimensional Hilbert space, denoted by  $|q\rangle = \begin{pmatrix} a \\ b \end{pmatrix} = a|0\rangle + b|1\rangle$  with  $|0\rangle = \begin{pmatrix} 1 \\ 0 \end{pmatrix}$  and  $|1\rangle = \begin{pmatrix} 0 \\ 1 \end{pmatrix}$ , where complex numbers  $a$  and  $b$  satisfy the normalization condition  $|a|^2 + |b|^2 = 1$ . Here, the orthonormal basis  $\{|0\rangle, |1\rangle\}$  of the Hilbert space corresponds to the values  $\{0, 1\}$  of a bit in classical computers. A quantum computing task is implemented by a *quantum circuit*, which is mathematically represented by a  $2^n \times 2^n$  unitary matrix  $U$ , i.e.,  $U^\dagger U = U U^\dagger = I_n$ , where  $U^\dagger$  is the (entry-wise) conjugate transpose of  $U$  and  $I_n$  is the identity matrix on  $\mathcal{H}$ . For an input  $n$ -qubit datum  $|\psi\rangle$ , the output of the circuit is a datum of the same size:  $|\psi'\rangle = U|\psi\rangle$ .

Like its classical counterpart, a quantum circuit  $U$  consists of a sequence (product) of *quantum logic gates*  $U_i$ , i.e.,  $U = U_d \cdots U_1$ . Here  $d$  is the gate number of the circuit  $U$ . Each gate  $U_i$  only non-trivially operates on one or two qubits. Fig. 2 shows an example of a 2-qubit quantum circuit for the QAOA algorithm.

$$\begin{array}{c} \bullet \\ \text{---} \\ \square \\ \text{---} \end{array} = \begin{pmatrix} 1 & 0 & 0 & 0 \\ 0 & 1 & 0 & 0 \\ 0 & 0 & u_{00} & u_{01} \\ 0 & 0 & u_{10} & u_{11} \end{pmatrix} \quad \begin{array}{c} \text{---} \\ \bullet \\ \text{---} \\ \bullet \\ \text{---} \end{array} = \begin{pmatrix} 1 & 0 & 0 & 0 \\ 0 & 1 & 0 & 0 \\ 0 & 0 & 1 & 0 \\ 0 & 0 & 0 & -1 \end{pmatrix}$$

**Quantum Noises:** In the current NISQ era, quantum noise is unavoidable, so we have to consider the noisy effect in quantum computing. Consequently, the uncertainty will be brought such that quantum states become mixed instead of pure states. A *mixed state* is considered as an ensemble

$\{(p_k, |\psi_k\rangle)\}$ , meaning the quantum system is in state  $|\psi_k\rangle$  with probability  $p_k$ . Mathematically, it can be described by a  $2^n \times 2^n$  density matrix  $\rho$  (Hermitian positive semi-definite matrix with unit trace<sup>1</sup>) on  $\mathcal{H}$ :  $\rho = \sum_k p_k |\psi_k\rangle\langle\psi_k|$ , where  $\langle\psi_k|$  is the conjugate transpose of  $|\psi_k\rangle$ , i.e.,  $\langle\psi_k| = |\psi_k\rangle^\dagger$ . In this situation, a computational task starting at a mixed state  $\rho$  is finished by a mapping  $\mathcal{E}$ :  $\rho' = \mathcal{E}(\rho)$ , where  $\mathcal{E}$  is a quantum channel. A channel  $\mathcal{E}$  (also called a *super-operator*) admits a *Kraus matrix form* [37]: there exists a finite set  $\{E_k\}_{k \in \mathcal{K}}$  of matrices on  $\mathcal{H}$  such that

$$\mathcal{E}(\rho) = \sum_{k \in \mathcal{K}} E_k \rho E_k^\dagger \quad \text{with} \quad \sum_{k \in \mathcal{K}} E_k^\dagger E_k = I_n,$$

where  $\{E_k\}_{k \in \mathcal{K}}$  is called *Kraus matrices* of  $\mathcal{E}$ . Specifically, quantum gate  $U$  can be viewed as a unitary channel where  $\mathcal{E}(\rho) = U\rho U^\dagger$ . Briefly,  $\mathcal{E}$  is represented as  $\mathcal{E} = \{E_k\}_{k \in \mathcal{K}}$ . Quantum noises can be described as quantum channels. A typical example of quantum noise is depolarizing noise, which is represented by the set of operators  $\{\sqrt{1-p}I, \sqrt{\frac{p}{3}}X, \sqrt{\frac{p}{3}}Y, \sqrt{\frac{p}{3}}Z\}$ . In this paper, we also adopt a decoherence noise model derived from superconducting circuits [38]. This model captures the decoherence effects arising from the interaction of the quantum system with its surrounding environment, which is a dominant source of noise in superconducting hardware. Mathematically, decoherence manifests as the decay of off-diagonal elements in the density matrix of mixed states, resulting from amplitude damping and phase damping.

- 1) **Amplitude Damping ( $\mathcal{E}_a$ ):** Amplitude damping describes the gradual loss of energy from excited states. It is characterized by the following Kraus operators:

$$E_{a,1} = \begin{pmatrix} 1 & 0 \\ 0 & e^{-\Delta t/2T_1} \end{pmatrix}, E_{a,2} = \begin{pmatrix} 0 & \sqrt{1 - e^{-\Delta t/T_1}} \\ 0 & 0 \end{pmatrix}$$

where  $T_1$  is the energy relaxation time and  $\Delta t$  is the gate time [38].

- 2) **Phase Damping ( $\mathcal{E}_p$ ):** Phase damping refers to pure dephasing, where the off-diagonal elements of the density matrix decay without affecting the diagonal elements. It is represented by the following Kraus operators:

$$\begin{aligned} E_{p,0} &= e^{-\Delta t/2T_\varphi} I, \\ E_{p,1} &= \sqrt{1 - e^{-\Delta t/T_\varphi}} |0\rangle\langle 0|, \\ E_{p,2} &= \sqrt{1 - e^{-\Delta t/T_\varphi}} |1\rangle\langle 1|, \end{aligned}$$

where  $T_\varphi$  is defined as  $\frac{1}{T_\varphi} = \frac{1}{T_2} - \frac{1}{2T_1}$ , and  $T_2$  is the total dephasing time [38].

The overall decoherence noise, denoted by  $\mathcal{E}_D$ , is the composition of amplitude damping and phase damping:

$$\mathcal{E}_D = \mathcal{E}_p \circ \mathcal{E}_a.$$

Similar to a noiseless quantum circuit  $U$ , a noisy quantum circuit  $\mathcal{E}$  also consists of a sequence of noisy gates  $\{\mathcal{E}_i\}$ , i.e.,  $\mathcal{E} = \mathcal{E}_d \circ \dots \circ \mathcal{E}_1$ , where each  $\mathcal{E}_i$  is either a noiseless gate or a noise channel.

<sup>1</sup> $\rho$  has unit trace if  $\text{tr}(\rho) = 1$ , where trace  $\text{tr}(\rho)$  of  $\rho$  is defined as the summation of diagonal elements of  $\rho$ .

**Tensor Network:** As mentioned in Section. I, the tensor network method is widely used in the (noisy) simulation of quantum circuits. For a better understanding, let us explain tensor network contraction by tensor diagram notation in the context of quantum circuits (see [39] for more details). Briefly, a tensor is a multi-dimensional array of complex numbers and is a labeled box with zero or more open output legs. Each leg labeled by an index (e.g.,  $i, j, k$ ) represents a dimension of the array, and a complex number is a tensor without legs. For example, the following notations represent a complex number (e.g.,  $e^{i\pi/4}$ ), a vector (e.g., pure state  $|\psi\rangle$ ), a matrix (e.g., quantum gate  $U$ ), respectively.

$$\boxed{e^{i\pi/4}} \quad j - \boxed{|\psi\rangle} \quad i - \boxed{U} - j$$

Furthermore, a tensor network is a graph where tensors act as nodes. These tensors can be contracted by connecting their legs that share the same indices. This operation, known as *tensor network contraction*, generalizes matrix (and vector) multiplication. For instance, the vector-matrix-vector product, given by  $\langle\phi|U|\psi\rangle = \sum_{ij} a_i U_{ij} b_j$  for  $|\phi\rangle = (a_1, \dots, a_{2^n})^\dagger$  and  $|\psi\rangle = (b_1, \dots, b_{2^n})^\top$ , and matrix-matrix product  $(AB)_{ik} = \sum_j A_{ij} B_{jk}$  are illustrated as the following two tensor contractions: All quantum circuits in the previous sections can be

$$\boxed{\langle\phi|} \overset{i}{-} \boxed{U} \overset{j}{-} \boxed{|\psi\rangle} = \boxed{\langle\phi|U|\psi\rangle}$$

$$i - \boxed{A} \overset{j}{-} \boxed{B} - k = i - \boxed{AB} - k$$

easily represented as tensor networks, where a gate is a tensor, and each leg of the gate is labeled by an index in  $\{0, 1\}$ .

One key advantage of representing quantum circuits as tensor networks is their ability to exploit the regularity and locality inherent in quantum circuit structures—features that matrix representations fail to capture effectively. Although the worst-case complexity grows exponentially with the depth of quantum circuit  $d^2$ , numerous efficient algorithms have been developed to perform tensor network contraction for large-scale practical quantum circuits, significantly mitigating this cost (e.g., [17, 18, 19, 20, 21]).

### III. NOISY QUANTUM CIRCUIT SIMULATION

The simulation task for a noiseless quantum circuit involves computing the state vector representation of the circuit's output state given an initial input state. For noisy quantum circuits, the simulation task instead aims to estimate the density matrix of the output state. Specifically, given a noisy quantum circuit  $\mathcal{E}_N$  and an input state  $\rho_0$ , the goal is to estimate  $\mathcal{E}_N(\rho_0)$ . The density matrix  $\mathcal{E}_N(\rho_0)$  is a  $2^n \times 2^n$  complex matrix. However, in practice, it is often unnecessary to store all of its elements

<sup>2</sup>The complexity of contracting a tensor network corresponding to a  $q$ -local-interacting quantum circuit is given by  $T^{O(1)} \exp[O(qd)]$  where  $T$  is the number of gates (tensors),  $d$  is the circuit depth, and a circuit is  $q$ -local-interacting if, under a linear ordering of qubits, each gate acts only on qubits within a distance of  $q$  [40].

explicitly. Instead, many applications require only statistical values obtained from measurements of the state.

In this paper, we focus on simulating the measurement probability of a quantum state, where the measurement is defined by a state  $|v\rangle$ , as formalized in Problem 1. This setting aligns with current test and verification algorithm frameworks and is widely adopted in hardware experiments. For example, in ATPG of quantum circuits [41], quantum gates are discriminated by choosing two states  $|w\rangle$  and  $|w'\rangle$ , followed by measurements defined by  $|w\rangle\langle w|$  and  $|w'\rangle\langle w'|$  on the output state separately.

**Problem 1** (Noisy Simulation Task of Quantum Circuits). *Given a noisy quantum circuit with depth  $d$  represented as  $\mathcal{E}_{\mathcal{N}} = \mathcal{E}_d \circ \dots \circ \mathcal{E}_1$  [37], an input state  $|\psi\rangle$ , and a measurement state  $|v\rangle$ , the noisy simulation task of  $\mathcal{E}_{\mathcal{N}}$  on  $|\psi\rangle$  is to estimate the probability  $\langle v | \mathcal{E}_{\mathcal{N}}(|\psi\rangle\langle\psi|) | v \rangle$  with high accuracy.*

Every entry of  $\mathcal{E}_{\mathcal{N}}(\rho_0)$  can be independently estimated by computing  $\langle x | \mathcal{E}_{\mathcal{N}}(\rho_0) | y \rangle$ , where  $|x\rangle, |y\rangle$  are pure states chosen from the computational basis of  $\mathcal{H}$ . Furthermore, solving Problem 1 allows us to compute these entries efficiently, as they can be expressed as:

$$\begin{aligned} \langle x | \mathcal{E}_{\mathcal{N}}(\rho_0) | y \rangle &= \frac{1}{4} \left( (\langle x | + \langle y |) \mathcal{E}_{\mathcal{N}}(\rho_0) (|x\rangle + |y\rangle) \right. \\ &\quad - (\langle x | - \langle y |) \mathcal{E}_{\mathcal{N}}(\rho_0) (|x\rangle - |y\rangle) \\ &\quad - i(\langle x | - i\langle y |) \mathcal{E}_{\mathcal{N}}(\rho_0) (|x\rangle + i|y\rangle) \\ &\quad \left. + i(\langle x | + i\langle y |) \mathcal{E}_{\mathcal{N}}(\rho_0) (|x\rangle - i|y\rangle) \right). \end{aligned} \quad (1)$$

This paper aims to solve Problem 1 using tensor networks as the data structure for modeling quantum circuits and SVD for approximating the tensor representation of quantum noise. In the following, we introduce a tensor network diagram for the noisy simulation task in Problem 1, which is the foundation for our approximation simulation algorithm. Furthermore, this diagram directly leads to a tensor network-based algorithm for exactly computing  $\langle v | \mathcal{E}_{\mathcal{N}}(|\psi\rangle\langle\psi|) | v \rangle$ .

Before presenting our noisy simulation method, we start with a trivial calculating method to show the usage of the tensor network in the simulation of noisy quantum circuits. By the Karus matrices of the quantum noise,  $\langle v | \mathcal{E}_{\mathcal{N}}(\psi) | v \rangle$  can be expanded into the following equations:

$$\langle v | \mathcal{E}_{\mathcal{N}}(\psi) | v \rangle \quad (2)$$

$$= \langle v | \mathcal{E}_d \circ \dots \circ \mathcal{E}_1(\psi) | v \rangle \quad (3)$$

$$= \sum_{k_1 \in \mathcal{K}_1} \dots \sum_{k_d \in \mathcal{K}_d} \langle v | E_{dk_d} \dots E_{1k_1} | \psi \rangle \langle \psi | E_{1k_1}^\dagger \dots E_{dk_d}^\dagger | v \rangle \quad (4)$$

$$= \sum_{k_1, \dots, k_d} \langle v | E_{dk_d} \dots E_{1k_1} | \psi \rangle (\langle v | E_{dk_d} \dots E_{1k_1} | \psi \rangle)^* \quad (5)$$

The above equations show a tensor network-based method to complete the simulation task in Problem 1. Specifically, we can substitute each super-operator in the circuit  $\mathcal{E}_{\mathcal{N}}$  with one of its Kraus matrices, and convert  $\langle v | E_{dk_d} \dots E_{1k_1} | \psi \rangle$  into a tensor network. Then the simulation result is the summation shown in Eq.(5). The key drawback of this tensor network-based method is that  $4^N$  tensor networks need to be contracted

where  $N$  is the number of noises in the simulated noisy circuit. The exponential cost on  $N$  leads to the fact that only noisy quantum circuits with very limited numbers of noise can be handled when simulating NISQ quantum circuits.

**Tensor Network Diagram for Noisy Simulation:** Instead of calculating each term separately in Eq. (5), an alternative way to compute  $\langle v | \mathcal{E}_{\mathcal{N}}(\psi) | v \rangle$  is as follows by using the matrix representation of quantum super-operators [42, Chapter 2.2.2].

$$\begin{aligned} \langle v | \mathcal{E}_{\mathcal{N}}(\psi) | v \rangle &= \text{tr}(|v\rangle\langle v | \mathcal{E}_{\mathcal{N}}(\psi)) \\ &= \langle \Omega | [ |v^*\rangle\langle v^* | \otimes \mathcal{E}_{\mathcal{N}}(\psi) ] | \Omega \rangle \\ &= \langle \Omega | [ |v^*\rangle\langle v^* | \otimes \mathcal{E}_d \circ \dots \circ \mathcal{E}_1(\psi) ] | \Omega \rangle \\ &= \langle v | \otimes \langle v^* | (M_{\mathcal{E}_d} \dots M_{\mathcal{E}_1}) | \psi \rangle \otimes | \psi^* \rangle \end{aligned}$$

where  $|v^*\rangle$  is the entry-wise conjugate of  $|v\rangle$ ,  $|\Omega\rangle$  is the (unnormalized) maximal entangled state, i.e.,  $|\Omega\rangle = \sum_j |j\rangle \otimes |j\rangle$  with  $\{|j\rangle\}$  being an orthonormal basis of Hilbert space  $\mathcal{H}$ , and  $M_{\mathcal{E}} = \sum_k E_k \otimes E_k^*$  for  $\mathcal{E} = \{E_k\}$  is called the *matrix representation* of  $\mathcal{E}$ . This representation can be visualized by the tensor network notation. For simplicity, we illustrate this on a one-qubit circuit which only consists of one noise. The trivial calculation method in Eq (5) corresponds to the tensor network on the left of Fig. 3. We can rotate the dashed part of the tensor network and get a tensor network as illustrated on the right side of Fig. 3.

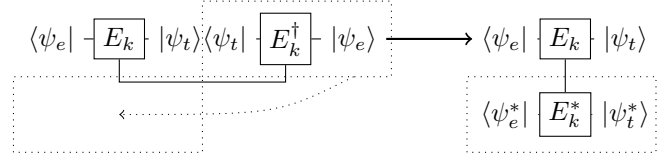


Fig. 3: New Tensor Network Diagram for Noisy Simulation

We observe that  $M_{\mathcal{E}} = \sum_{k \in \mathcal{K}} E_k \otimes E_k^*$  represents the noises in the newly obtained tensor network. In particular, for a unitary  $U = \{U\}$ ,  $M_U$  is depicted as the tensor network in the following.

$$\begin{aligned} M_{\mathcal{E}} &= \sum_{k \in \mathcal{K}} E_k \otimes E_k^* = \begin{array}{c} \boxed{E_k} \\ | \\ \boxed{E_k^*} \end{array} \\ M_U &= U \otimes U^* = \begin{array}{c} \boxed{U} \\ | \\ \boxed{U^*} \end{array} \end{aligned}$$

With this observation, we get a serial connection of the two tensor networks representing  $n$ -qubit circuits  $\mathcal{E}_{\mathcal{N}}$ . Subsequently, we can compute  $\langle v | \otimes \langle v^* | (M_{\mathcal{E}_d} \dots M_{\mathcal{E}_1}) | \psi \rangle \otimes | \psi^* \rangle$  by contracting a tensor network with double size ( $2n$  qubits). An illustration of the tensor network diagram of the two-qubit QAOA circuit mentioned in Sec. II is shown in Fig. 4. Based on this idea, an algorithm (Algorithm 1) can be used to compute  $\langle v | \mathcal{E}_{\mathcal{N}}(\psi) | v \rangle$ . When we contract tensor networks, splitting is a standard technique that cuts some edges and converts the task of contracting a large tensor network into contracting a set of smaller tensor networks. Algorithm 1 is the same as the direct computational method if we cut all vertical edges of the tensor representation of  $M_{\mathcal{E}}$ . However, the double-size tensor network enables tensor network contraction tools

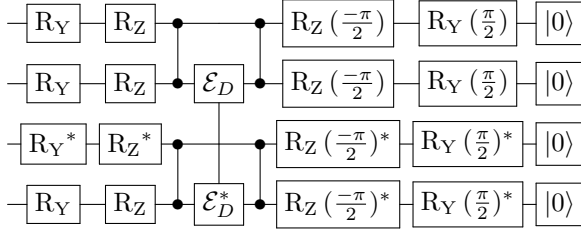


Fig. 4: Circuit for noisy simulation of the 2-qubit QAOA circuit in Fig. 2 with decoherence noise  $\mathcal{E}_D$  by appending  $|v\rangle = U|\psi\rangle$  to the end of the circuit, and redundant gates are canceled out.

to find other more efficient contraction strategies that may be better than the trivial method in Eq.(5).

---

**Algorithm 1** NoiseSimulation( $\mathcal{E}_N, |\psi\rangle, |v\rangle$ )

---

**Input:** A noisy quantum circuit  $\mathcal{E}_N = \mathcal{E}_d \circ \dots \circ \mathcal{E}_1$  with  $\mathcal{E}_i = \{E_{ik}\}_{k \in \mathcal{K}_i}$  for  $1 \leq i \leq d$ , a test state  $|\psi\rangle$  and an expected output  $|v\rangle$ .

**Output:** Noisy simulation result  $\langle v | \mathcal{E}_N(\psi) | v \rangle$

- 1: Computing  $X = \langle v | \otimes \langle v^* | (M_{\mathcal{E}_d} \dots M_{\mathcal{E}_1}) | \psi \rangle \otimes | \psi^* \rangle$  by calling a tool for tensor network contraction
  - 2: **return** X
- 

#### IV. APPROXIMATION ALGORITHM FOR NOISY QUANTUM CIRCUIT SIMULATION

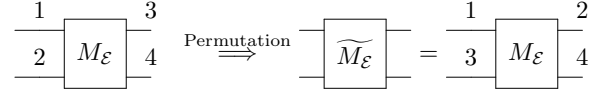
We are ready to present our approximation noisy simulation algorithm based on the tensor network diagram with the matrix representation of noises.

**Approximation Noisy Simulation Algorithm:** As we can see, the noises make simulating a quantum circuit much harder. To handle the difficulty of simulating a circuit with a large number of noises, we introduce an approximation noisy circuit simulation method based on the matrix representation and SVD, which can balance the accuracy and efficiency of the simulation. The insight of our method starts with an observation that most noises occurring in physical quantum circuits are close to the identity operators (matrices). Take the depolarizing noise as an example, which is defined by

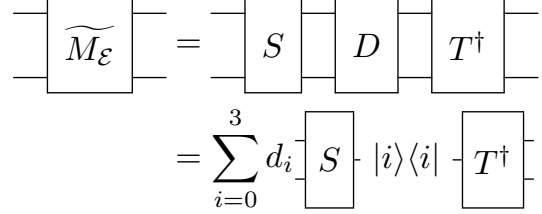
$$\mathcal{E}(\rho) = (1-p)\rho + \frac{p}{3}(X\rho X + Y\rho Y + Z\rho Z).$$

Probability  $p$  can be regarded as a metric of the noisy effectiveness of the channel. When  $p$  is small, the noise is almost identical to the identity channel. Therefore, a straightforward method is to approximately represent the depolarizing channel by  $(1-p)I$ . The current physical implementation of practical quantum algorithms requires that the effectiveness of noise is insignificant. For general noise  $\mathcal{E}$ , we define  $\|M_{\mathcal{E}} - I\|$  as the *noise rate* of  $\mathcal{E}$ , where  $\|\cdot\|$  is the 2-norm of matrix. For example, the depolarizing noise with parameter  $p$  has a noise rate  $2p$ . Next, we will describe our approximation algorithm and explain why it is efficient when the noise rate is small.

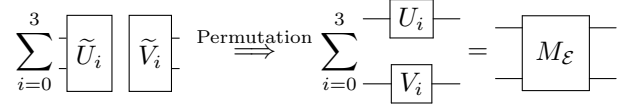
To handle the noises, we perform SVD on the matrix representation of each noise as illustrated in Fig. 5.



(a) Tensor Permutation



(b) SVD on  $\tilde{M}_{\mathcal{E}}$



(c) Tensor Permutation

Fig. 5: Decomposition of  $M_{\mathcal{E}}$

Suppose we treat  $M_{\mathcal{E}}$  as a tensor with rank 4, and the edges are indexed as in Fig. 5 (a).  $M_{\mathcal{E}}$  is the matrix with edges 1, 2 being the row and 3, 4 being the column. We introduce the tensor permutation operator where  $\tilde{M}_{\mathcal{E}}$  is the matrix with 1, 3 being the row and 2, 4 being the column. For example, the identity operator  $I$  on two qubits and its tensor permutation  $\tilde{I}$  are:

$$I = \begin{pmatrix} 1 & 0 & 0 & 0 \\ 0 & 1 & 0 & 0 \\ 0 & 0 & 1 & 0 \\ 0 & 0 & 0 & 1 \end{pmatrix} \quad \tilde{I} = \begin{pmatrix} 1 & 0 & 0 & 1 \\ 0 & 0 & 0 & 0 \\ 0 & 0 & 0 & 0 \\ 1 & 0 & 0 & 1 \end{pmatrix}$$

Performing SVD on  $\tilde{M}_{\mathcal{E}}$  we have  $\tilde{M}_{\mathcal{E}} = S D T^\dagger$ , where  $D = \sum_{i=0}^3 d_i |i\rangle\langle i|$  and  $d_0$  is the most significant singular value (see Fig. 5(b)). Let  $\tilde{U}_i = d_i S |i\rangle$  and  $\tilde{V}_i = T |i\rangle$  as in the left of Fig. 5 (c), we get  $\tilde{M}_{\mathcal{E}} = \sum_{i=0}^3 \tilde{U}_i \tilde{V}_i^\dagger$ . Then use tensor permutation again on  $\tilde{U}_i$  and  $\tilde{V}_i$  (here  $\tilde{U}_i$  is treated as a rank 4 tensor with index 3, 4 being 0-dimension, and  $\tilde{V}_i$  is treated as a rank 4 tensor with index 1, 2 being 0-dimension), we get  $M_{\mathcal{E}} = \sum_{i=0,1,2,3} U_i \otimes V_i$ , as illustrated in Fig. 5 (c).

Next, we will show that when the noise rate of  $\mathcal{E}$  is small,  $U_0 \otimes V_0$  is a good approximation of  $M_{\mathcal{E}}$ .

**Lemma 1.** Suppose  $A$  and  $B$  are  $4 \times 4$  matrices, and  $\tilde{A}$  and  $\tilde{B}$  are the tensor permutation of  $A$  and  $B$  as defined before. If  $\|A - B\| < \delta$ , then we have  $\|\tilde{A} - \tilde{B}\| < 2\delta$ .

*Proof.* We use  $\|\cdot\|_F$  to denote the Frobenius norm of matrices. Specifically, for  $4 \times 4$  matrices, it can be shown that  $\|A\| \leq \|A\|_F \leq 2\|A\|$ . Note that  $A$  and  $\tilde{A}$  have the same Frobenius norm since the tensor permutation operator only rearranges the positions of elements. Therefore we have  $\|\tilde{A} - \tilde{B}\| \leq \|\tilde{A} - \tilde{B}\|_F = \|A - B\|_F \leq 2\|A - B\| < 2\delta$ .  $\square$

**Lemma 2.** Suppose  $\|M_{\mathcal{E}} - I\| < \delta$ , then we have  $\|M_{\mathcal{E}} - U_0 \otimes V_0\| < 4\delta$

*Proof.* By Lemma 1. we have  $\|\tilde{M}_{\mathcal{E}} - \tilde{I}\| < 2\delta$ . Suppose we perform SVD on  $\tilde{M}_{\mathcal{E}}$  we have  $\tilde{M}_{\mathcal{E}} = SDT^\dagger$ . And let  $D_0 = d_0|0\rangle\langle 0|$ , we have

$$\|\tilde{M}_{\mathcal{E}} - SD_0T^\dagger\| = \min_{\text{rank}(A)=1} \|\tilde{M}_{\mathcal{E}} - A\| \leq \|\tilde{M}_{\mathcal{E}} - \tilde{I}\| < 2\delta.$$

The first equation comes from the Eckart-Young-Mirsky theorem [43]. The last inequality holds because  $\tilde{I}$  has rank 1. And note that  $\tilde{M}_{\mathcal{E}} = M_{\mathcal{E}}$  and  $SD_0T^\dagger = U_0 \otimes V_0$ , by Lemma 1, we have

$$\|M_{\mathcal{E}} - U_0 \otimes V_0\| < 4\delta. \quad \square$$

We are ready to introduce our approximation algorithm for the noisy quantum circuit simulation task. Suppose  $\mathcal{E}_{\mathcal{N}} = \mathcal{E}_d \circ \dots \circ \mathcal{E}_1$  is a quantum circuit with  $N$  noises, where the noise channels have index  $\{i_1, \dots, i_N\}$ . After applying SVD on each matrix representation of noises we get  $M_{\mathcal{E}_{i_s}} = U_0^s \otimes V_0^s + U_1^s \otimes V_1^s + U_2^s \otimes V_2^s + U_3^s \otimes V_3^s$ ,  $s \in \{1, \dots, N\}$ , where  $M_{\mathcal{E}_{i_s}}$  is closed to  $U_0^s \otimes V_0^s$ . The idea of our algorithm is to calculate the simulation result by using  $U_0^s \otimes V_0^s$  to substitute the noises as a prior choice. Let  $M'_{\mathcal{E}_{i_s}} = U_0^s \otimes V_0^s$  and  $\overline{M_{\mathcal{E}_{i_s}}} = U_1^s \otimes V_1^s + U_2^s \otimes V_2^s + U_3^s \otimes V_3^s$ . Thus  $M_{\mathcal{E}_{i_s}} = M'_{\mathcal{E}_{i_s}} + \overline{M_{\mathcal{E}_{i_s}}}$  and  $\|\overline{M_{\mathcal{E}_{i_s}}}\| < 4\delta$  by Lemma 2. Let  $T_u$  be the sum of tensor networks obtained by substituting all but  $u$  noises to  $M'_{\mathcal{E}_{i_s}}$  and  $u$  noises to one of  $U_i^s \otimes V_i^s$ ,  $i = 1, 2, 3$ ,

i.e.,  $T_u = \sum_{1 \leq p_1 < \dots < p_u \leq N} \prod_{r=1}^u \overline{M_{\mathcal{E}_{i_{p_r}}}} \prod_{t \notin \{p_1, \dots, p_u\}} M'_{\mathcal{E}_{i_t}}$ . We call

$A(l) = \sum_{u=0}^l T_u$  the  $l$ -level approximation of  $\mathcal{E}_{\mathcal{N}}$ . By increasing the approximation level  $l$  we get a better approximation for  $\mathcal{E}_{\mathcal{N}}$ , when  $l = N$ ,  $A(l) = M_{\mathcal{E}_{\mathcal{N}}}$  exactly. Our algorithm is to calculate  $A(l)$  for a given  $l$ . Details of the algorithm are shown in Algorithm 2.

**Example 1** (Decomposition of Depolarizing Noise). *Here we illustrate our decomposition method by implementing our algorithm on depolarizing noise. Specifically, consider depolarizing noise with  $p = 0.01$ , i.e.  $\mathcal{E}(\rho) = 0.99\rho + \frac{1}{300}(X\rho X + Y\rho Y + Z\rho Z)$ . Our method is as follows:*

- 1) First, from the Kraus matrices of depolarizing noise, we can calculate the matrix representation of the depolarizing noise, which is

$$\begin{aligned} M_{\mathcal{E}} &= 0.99I \otimes I + \frac{1}{300}(X \otimes X + Y \otimes Y + Z \otimes Z) \\ &= \begin{pmatrix} 0.9933 & 0 & 0 & 0 \\ 0 & 0.9867 & 0.0067 & 0 \\ 0 & 0.0067 & 0.9867 & 0 \\ 0 & 0 & 0 & 0.9933 \end{pmatrix} \end{aligned}$$

- 2) We start our decomposition by performing tensor permutation first, which derives the matrix

$$\widetilde{M}_{\mathcal{E}} = \begin{pmatrix} 0.9933 & 0 & 0 & 0.9867 \\ 0 & 0 & 0.0067 & 0 \\ 0 & 0.0067 & 0 & 0 \\ 0.9867 & 0 & 0 & 0.9933 \end{pmatrix}$$

- 3) By performing SVD on the derived matrix  $\widetilde{M}_{\mathcal{E}}$  as illustrated in Fig. 5(b), we have  $\widetilde{M}_{\mathcal{E}}$ , where

$$\begin{aligned} S &= \begin{pmatrix} -0.7071 & 0.7071 & 0 & 0 \\ 0 & 0 & -1 & 0 \\ 0 & 0 & 0 & 1 \\ -0.7071 & -0.7071 & 0 & 0 \end{pmatrix} \\ D &= \begin{pmatrix} 1.98 & 0 & 0 & 0 \\ 0 & 0.0067 & 0 & 0 \\ 0 & 0 & 0.0067 & 0 \\ 0 & 0 & 0 & 0.0067 \end{pmatrix} \\ T &= \begin{pmatrix} -0.7071 & 0 & 0 & -0.7071 \\ 0.7071 & 0 & 0 & -0.7071 \\ 0 & 0 & -1 & 0 \\ 0 & 1 & 0 & 0 \end{pmatrix} \end{aligned}$$

- 4) Finally, by calculating  $\widetilde{U}_i$  and  $\widetilde{V}_i$ , and performing the tensor permutation once more, we complete the decomposition of  $M_{\mathcal{E}}$ .

$$\begin{aligned} M_{\mathcal{E}} &= 1.98 \begin{pmatrix} -0.707 & 0 \\ 0 & -0.707 \end{pmatrix} \otimes \begin{pmatrix} -0.707 & 0 \\ 0 & -0.707 \end{pmatrix} \\ &+ 0.0067 \begin{pmatrix} 0.707 & 0 \\ 0 & -0.707 \end{pmatrix} \otimes \begin{pmatrix} 0.707 & 0 \\ 0 & -0.707 \end{pmatrix} \\ &+ 0.0067 \begin{pmatrix} 0 & -1 \\ 0 & 0 \end{pmatrix} \otimes \begin{pmatrix} 0 & 0 \\ -1 & 0 \end{pmatrix} \\ &+ 0.0067 \begin{pmatrix} 0 & 0 \\ 1 & 0 \end{pmatrix} \otimes \begin{pmatrix} 0 & 1 \\ 0 & 0 \end{pmatrix} \end{aligned}$$

---

### Algorithm 2 ApproximationNoisySimulation( $\mathcal{E}_{\mathcal{N}}$ , $|\psi\rangle$ , $|v\rangle$ , $l$ )

---

**Input:** A noisy quantum circuit  $\mathcal{E}_{\mathcal{N}} = \mathcal{E}_d \circ \dots \circ \mathcal{E}_1$  with  $N$  noises, where the noise channels have index  $\{i_1, \dots, i_N\}$  and Kraus matrices  $\mathcal{E}_{i_s} = \{E_{sk}\}_{k \in \mathcal{K}_s}$  for  $1 \leq s \leq N$ , an input state  $|\psi\rangle$ , a measurement defined by state  $|v\rangle$  and a level for the approximation  $l$ .

**Output:**  $G^l = \langle v | \otimes \langle v^* | A(l) | \psi \rangle \otimes |\psi^*\rangle$ , the  $l$ -level approximation of  $\langle v | \mathcal{E}_{\mathcal{N}}(|\psi\rangle\langle\psi|) | v \rangle$

- 1: Result = 0
  - 2: Generate the tensor network as in the accuracy algorithm.
  - 3: Perform tensor permutation and SVD operation to the matrix representation of all noises  $M_{\mathcal{E}_{i_s}}$ , obtaining  $U_k^s$  and  $V_k^s$ , where  $M_{\mathcal{E}_{i_s}} = U_0^s \otimes V_0^s + U_1^s \otimes V_1^s + U_2^s \otimes V_2^s + U_3^s \otimes V_3^s$ ,  $s \in \{1, \dots, N\}$ .
  - 4: **for all**  $0 \leq k \leq l$  **do**
  - 5:     Calculate approximation of level  $k$ :
  - 6:      $R_k := 0$
  - 7:     **for all**  $1 \leq p_1 < \dots < p_k \leq N$  **do**
  - 8:         Substitute  $M_{\mathcal{E}_{i_{p_j}}}$  with one of  $U_1^{p_j} \otimes V_1^{p_j}, U_2^{p_j} \otimes V_2^{p_j}, U_3^{p_j} \otimes V_3^{p_j}$  for  $j \in \{1, \dots, k\}$ . For  $s \notin \{p_1, p_2, \dots, p_k\}$ , substitute  $M_{\mathcal{E}_{i_s}}$  to  $U_0^s \otimes V_0^s$ .
  - 9:         After substitution, the original (double-sized) tensor network is split into two tensor networks, contract both tensor networks, and multiply the result, donated as  $X$ .
  - 10:          $R_k += X$ .
  - 11:     **end for**
  - 12:     Result +=  $R_k$ .
  - 13: **end for**
  - 14: **return** Result
- 

**Theorem 1** (Precision and Complexity of Algorithm 2). *Given a noisy quantum circuits  $\mathcal{E}_{\mathcal{N}}$  with  $d$  gates and  $N$  noises with all noise rates being less than  $p$ , i.e.,  $\|M_{\mathcal{E}_{i_s}} - I\| < p$  for*

$s \in \{1, \dots, N\}, i_s \in \{1, \dots, d\}$ . For any input and output state  $|\psi\rangle$  and  $|v\rangle$ , donate the fidelity as  $G = \langle v | \mathcal{E}_{\mathcal{N}}(|\psi\rangle\langle\psi|) |v\rangle$ , and the approximation result is  $G' = \langle v | \otimes \langle v^* | A(l) |\psi\rangle \otimes |\psi^*\rangle$ , we have  $|G - G'| < (1 + 8p)^N - \sum_{i=0}^l \binom{N}{i} (4p)^i (1 + 4p)^{(N-i)}$ , and

the number of tensor network contractions is  $2 \sum_{i=0}^l \binom{N}{i} 3^i$ .

*Proof.* We first observe:

$$\begin{aligned} \|M_{\mathcal{E}_N} \cdots M_{\mathcal{E}_1} - A(l)\| &= \left\| \sum_{i=l+1}^N T_i \right\| \leq \sum_{i=l+1}^N \|T_i\| \\ &\leq \sum_{i=l+1}^N \binom{N}{i} (4p)^i (1 + 4p)^{(N-i)} \\ &= (1 + 8p)^N - \sum_{i=0}^l \binom{N}{i} (4p)^i (1 + 4p)^{(N-i)} \end{aligned}$$

Therefore

$$\begin{aligned} \|G - G'\| &= |\langle v | \otimes \langle v^* | (M_{\mathcal{E}_N} \cdots M_{\mathcal{E}_1} - A(l)) |\psi\rangle \otimes |\psi^*\rangle | \\ &\leq \| |v\rangle \otimes \langle v^* | \| \| (M_{\mathcal{E}_N} \cdots M_{\mathcal{E}_1} - A(l)) |\psi\rangle \otimes |\psi^*\rangle \| \\ &\leq \| (M_{\mathcal{E}_N} \cdots M_{\mathcal{E}_1} - A(l)) \| \\ &= (1 + 8p)^N - \sum_{i=0}^l \binom{N}{i} (4p)^i (1 + 4p)^{(N-i)} \end{aligned}$$

Fixing all but  $i$  factors into the form " $U_0 \otimes V_0$ " results in a contraction number of  $2 \binom{N}{i} 3^i$ , therefore the total number of tensor network contractions is  $2 \sum_{i=0}^l \binom{N}{i} 3^i$ .  $\square$

Specifically, when using the one-level approximation where the number of noises is  $N$  and the noise rate is  $p$ , Theorem 1 asserts that our method has accuracy  $(1 + 8p)^N - (1 + 4p)^N - 4Np(1 + 4p)^{N-1}$ . With the assumption that  $p \leq \frac{1}{8N}$ , we have

$$\begin{aligned} &(1 + 8p)^N - (1 + 4p)^N - 4Np(1 + 4p)^{N-1} \\ &= \sum_{k=2}^N \binom{N}{k} (4p)^k (1 + 4p)^{N-k} \\ &\leq (1 + \frac{1}{2N})^N \sum_{k=2}^N (4Np)^k \\ &\leq \sqrt{e} (4Np)^2 \frac{1 - (4Np)^{N-1}}{1 - 4Np} \\ &\leq 32\sqrt{e} N^2 p^2 \end{aligned}$$

As a comparison, the quantum trajectories method [16, 26] needs  $r$  samples (tensor network contraction) to obtain a result within accuracy  $O(1/\sqrt{r})$  under a constant possibility. For the quantum trajectories method to achieve such accuracy (under a constant probability),  $N^2 p^2 = \frac{C}{\sqrt{r}}$ . Therefore the sample number  $r = \frac{C^2}{N^4 p^4}$ , where  $C$  is a constant number. Note that our level-1 approximation needs  $O(N)$  samples, and therefore our approximation method will need less sampling number than the Monte-Carlo method when  $p = O(N^{-\frac{3}{4}})$ .

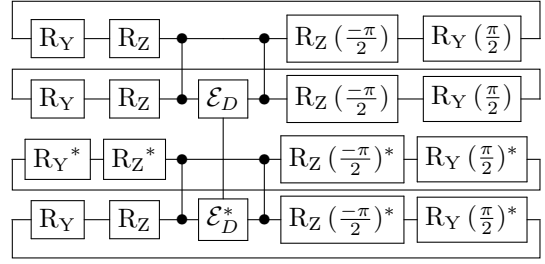


Fig. 6: Tensor network for equivalence checking of the 2-qubit QAOA circuit in Fig. 2 with decoherence noise  $\mathcal{E}_D$ , and redundant gates are canceled out.

## V. APPLICATIONS IN EQUIVALENCE CHECKING

The method developed in the last section can also be used in equivalence checking of noisy quantum circuits. Since quantum circuits are affected by noise, instead of determining whether two quantum circuits are exactly equivalent, it is more practical to verify if two circuits are approximately equivalent with certain degree. The equivalence degree of two noisy quantum circuits can be defined using the Jamiolkowski fidelity of their corresponding super-operators [44]. Let  $|\Psi\rangle = \frac{1}{\sqrt{d}} \sum_i |ii\rangle$  be the maximally entangled state. For each super-operator  $\mathcal{E}$  on  $\mathcal{H}$ ,  $\rho_{\mathcal{E}} = (\mathcal{I} \otimes \mathcal{E})(|\Psi\rangle\langle\Psi|)$ , where  $\mathcal{I}$  is the identity super-operator on  $\mathcal{H}$ .

**Definition 1** (Jamiolkowski fidelity). *The Jamiolkowski fidelity between super-operators  $\mathcal{E}$  and  $\mathcal{F}$  is defined as*

$$F_J(\mathcal{E}, \mathcal{F}) = F(\rho_{\mathcal{E}}, \rho_{\mathcal{F}}).$$

As shown in [34], the Jamiolkowski fidelity between a noisy channel and a unitary channel can be calculated by

$$F_J(\mathcal{U}, \mathcal{E}_{\mathcal{N}}) = \frac{1}{2^N} \text{Tr}((U^\dagger \otimes U^T) M_{\mathcal{E}})$$

This calculation can be converted to the contraction of a tensor network using twice the number of qubits as the original circuit. Fig. 6 shows the tensor network for equivalence checking of the quantum circuit shown in Fig. 2. Based on the tensor network representation, we can also implement our approximation method to derive an approximate equivalence checking algorithm. Details of the algorithm are shown in Algorithm. 3. The precision and complexity of the algorithm are analyzed in the Theorem. 2

**Theorem 2** (Precision and Complexity of Algorithm 3). *Given a noisy quantum circuits  $\mathcal{E}_{\mathcal{N}}$  with  $d$  gates and  $N$  noises with all noise rates being less than  $p$ , i.e.,  $\|M_{\mathcal{E}_{i_s}} - I\| < p$  for  $s \in \{1, \dots, N\}, i_s \in \{1, \dots, d\}$ . We have  $|F_J(\mathcal{U}, \mathcal{E}_{\mathcal{N}}) - F(l)| < (1 + 8p)^N - \sum_{i=0}^l \binom{N}{i} (4p)^i (1 + 4p)^{(N-i)}$ , and also the number of tensor network contractions is  $2 \sum_{i=0}^l \binom{N}{i} 3^i$ .*

*Proof.* Since

$$\begin{aligned} &|\text{Tr}((U^\dagger \otimes U^T) M_{\mathcal{E}}) - \text{Tr}((U^\dagger \otimes U^T) M_{\mathcal{E}_T})| \\ &= |\text{Tr}((U^\dagger \otimes U^T) (M_{\mathcal{E}} - M_{\mathcal{E}_T}))| \end{aligned}$$



**Algorithm 3** ApproximationEquivalenceChecking( $\mathcal{E}_N, U, l$ )

---

**Input:** An ideal circuit  $U = U_d \circ \dots \circ U_1$ , and the noisy quantum circuit  $\mathcal{E}_N = \mathcal{E}_d \circ \dots \circ \mathcal{E}_1$  with  $N$  noises, where the noise channels have index  $\{i_1, \dots, i_N\}$  and Kraus matrices  $\mathcal{E}_{i_s} = \{E_{sk}\}_{k \in \mathcal{K}_s}$  for  $1 \leq s \leq N$ .

**Output:**  $F(l)$ , the  $l$ -level approximation of  $F_J(U, \mathcal{E}_N)$

- 1: Result = 0
- 2: Generate the tensor network similar with the tensor network in algorithm 2, where the start and the end of each qubit is connected to compute the trace.
- 3: Perform tensor permutation and SVD operation to the matrix representation of all noises  $M_{\mathcal{E}_{i_s}}$ , obtaining  $U_k^s$  and  $V_k^s$ , where  $M_{\mathcal{E}_{i_s}} = U_0^s \otimes V_0^s + U_1^s \otimes V_1^s + U_2^s \otimes V_2^s + U_3^s \otimes V_3^s$ ,  $s \in \{1, \dots, N\}$ .
- 4: **for all**  $0 \leq k \leq l$  **do**
- 5:     Calculate approximation of level  $k$ :
- 6:      $T_k := 0$
- 7:     **for all**  $1 \leq p_1 < \dots < p_k \leq N$  **do**
- 8:         Substitute  $M_{\mathcal{E}_{i_{p_j}}}$  with one of  $U_1^{p_j} \otimes V_1^{p_j}, U_2^{p_j} \otimes V_2^{p_j}, U_3^{p_j} \otimes V_3^{p_j}$  for  $j \in \{1, \dots, k\}$ . For  $s \notin \{p_1, p_2, \dots, p_k\}$ , substitute  $M_{\mathcal{E}_{i_s}}$  to  $U_0^s \otimes V_0^s$ .
- 9:         After substitution, the original (double-sized) tensor network is split into two tensor networks, contract both tensor networks, and multiply the result, denoted as  $X$ .
- 10:          $T_k += X$ .
- 11:     **end for**
- 12:     Result +=  $T_k$ .
- 13: **end for**
- 14: **return** Result

---

By Cauchy–Schwarz inequality we have:

$$\begin{aligned}
& |\text{Tr}((U^\dagger \otimes U^T)(M_{\mathcal{E}} - M_{\mathcal{E}_T}))|^2 \\
&= \langle U \otimes U^*, M_{\mathcal{E}} - M_{\mathcal{E}_T} \rangle_{HS} \\
&\leq \|U \otimes U^*\|^2 \|M_{\mathcal{E}} - M_{\mathcal{E}_T}\|^2 \\
&\leq \|U \otimes U^*\|_F^2 \|M_{\mathcal{E}} - M_{\mathcal{E}_T}\|_F^2 \\
&= 2^{2N} \|M_{\mathcal{E}} - M_{\mathcal{E}_T}\|_F^2
\end{aligned}$$

Therefore we have

$$\begin{aligned}
& |F_J(U, \mathcal{E}_N) - F(l)| \\
&\leq \frac{1}{2^N} \cdot 2^N \|M_{\mathcal{E}} - M_{\mathcal{E}_T}\|_F \\
&= (1 + 8p)^N - \sum_{i=0}^l \binom{N}{i} (4p)^i (1 + 4p)^{(N-i)}
\end{aligned}$$

The total contraction number is same as analyzed in Theorem 1.  $\square$

## VI. EXPERIMENTS

In this section, we demonstrate the utility and effectiveness of our approximation approach. We evaluate our methods by performing noisy simulation and equivalence checking on various quantum circuits with realistic noise models. In particular, we compare our algorithm with state-of-the-art methods for the same tasks, and further numerically analyze our algorithm in terms of efficiency, accuracy, approximation levels, and noise rate. The code of our implementation can be accessed at the GitHub repository.<sup>3</sup>

<sup>3</sup><https://github.com/Veri-Q/NoiseSim>

### A. Experiment Configurations:

1) *Hardware and Software Tools:* All our experiments are carried out on a server with Intel Xeon Platinum 8153 @ 2.00GHz  $\times$  256 Cores, 2048 GB Memory. The machine runs CentOS 7.7.1908. We use the Google TensorNetwork Python package [15] for the tensor network computation. The memory out (MO) limit is capped at 2048 GB.

2) *Benchmark Circuits:* Our benchmark circuits consist of five types of quantum circuits: Bernstein-Vazirani (BV) Algorithm, Quantum Fourier Transform (QFT), Quantum Approximate Optimization Algorithm (QAOA), Hartree-Fock Variational Quantum Eigensolver (VQE), and random quantum circuits exhibiting quantum supremacy from Google (inst). Google has experimentally run the last three types of quantum circuits on their quantum processors. In our experiments, the benchmark circuits for BV and QFT are taken from [45], and the benchmark circuits for VQE, QAOA and inst are taken from ReCirq [46], an open-source library for Cirq and Google’s Quantum Computing Service.

3) *Noise Models:* Our method can handle any noise represented by a super-operator. To evaluate its performance, we consider two noise models. The first is depolarizing noise, a fundamental noise model commonly evaluated in most methods. This allows for a fair comparison of performance across different approaches. The other is the decoherence noise explained in Section II. In our experiments, the default decoherence times are set to  $T_1 = 200 \mu\text{s}$  and  $T_2 = 30 \mu\text{s}$ . The decoherence noise is applied after a randomly selected gate in the quantum circuit. While more complex than depolarizing noise, the decoherence noise model approximates the real noise effects in superconducting quantum circuits. By evaluating our approximation algorithm on benchmark circuits with this noise model, we obtain a practical assessment of its accuracy and efficiency in simulating the implementation of quantum algorithms on NISQ devices.

4) *Parallel Optimization:* Our approximation algorithm exhibits inherent parallelism as multiple subtasks of contraction can be executed independently. We implement parallel computing through Python’s multiprocessing package to accelerate result computation. For quantum circuits with limited scale (e.g., fewer qubits and gates), this parallelization strategy achieves significant speedup by fully utilizing multi-core CPU resources. However, when handling large-scale quantum circuits, the memory consumption of each subtask approaches the system’s physical memory limit, causing diminishing returns from parallelization as computational resources become saturated. While utilizing GPU could enhance performance, the critical memory (VRAM) bottleneck makes CPU-based computation our preferred choice, as it provides substantially larger addressable memory space to support the simulation of larger tensor networks. Finally, we employ a heuristic strategy that adjusts the number of processes based on the number of qubits and gates in the circuit, balancing efficiency with memory limitations.

5) *Baselines:* To evaluate the performance of our approximation algorithm, we compare it against state-of-the-art methods for simulating and verifying the equivalence of

TABLE I: OUR ALGORITHM VS. ACCURATE METHODS

Type	Qubits	Gates	Depth	Simulation							Equivalence Checking		
				#Noise = 2				#Noise = 20			#Noise = 20		
				MM	TDD	DDSIM	TN	Ours	TN	Ours	TDD	TN	Ours
BV	500	1499	502	MO	17.53	-	22.28	<b>19.94</b>	139.26	<b>47.83</b>	17.53	22.28	<b>19.94</b>
	10000	29999	10002	MO	108.94	-	131.84	<b>118.39</b>	692.4	<b>182.94</b>	108.94	131.84	<b>118.39</b>
QFT	10	235	69	28.39	164.83	160.11	0.33	<b>0.28</b>	23.74	<b>12.48</b>	164.83	23.74	<b>12.48</b>
	35	3010	271	MO	TO	TO	2490.68	<b>824.39</b>	MO	<b>6342.37</b>	TO	2490.68	<b>824.39</b>
HF-VQE	6	155	72	0.17	1.2	15.21	0.095	<b>0.084</b>	0.093	<b>0.52</b>	4.84	3.06	<b>3.78</b>
	8	308	124	0.24	3.65	17.3	0.33	<b>0.17</b>	0.31	<b>0.73</b>	10.48	2.15	<b>2.64</b>
	10	461	142	26.91	7.59	7.73	0.39	<b>0.38</b>	0.39	<b>0.49</b>	4.22	2.84	<b>2.34</b>
	12	690	194	206.37	18.81	9.44	0.99	<b>0.53</b>	0.98	<b>0.86</b>	3.85	1.5	<b>1.03</b>
QAOA	64	1696	42	MO	58.33	213.77	3.51	<b>3.11</b>	47.38	<b>28.25</b>	TO	1232.21	<b>2709.46</b>
	121	3322	42	MO	225.76	-	9.77	<b>8.96</b>	1131.61	<b>348.75</b>	TO	5033.26	<b>4897.58</b>
	225	6330	42	MO	MO	-	925.87	<b>822.54</b>	MO	<b>5294.47</b>	TO	MO	<b>8496.4</b>
Supremacy	16	115	11	MO	0.88	566.49	0.07	<b>0.05</b>	0.08	<b>0.25</b>	118.38	18.9	<b>6.23</b>
	16	394	41	MO	TO	TO	4.34	<b>6.3</b>	MO	<b>44.32</b>	TO	152.46	<b>9.03</b>
	16	764	81	MO	TO	TO	11.26	<b>9.53</b>	MO	<b>83.49</b>	TO	MO	<b>30.85</b>
	20	145	11	MO	1.52	TO	0.1	<b>0.14</b>	0.1	<b>0.33</b>	TO	MO	<b>78.4</b>
	20	261	21	MO	TO	TO	0.3	<b>0.28</b>	3725.2	<b>62.95</b>	193.64	130.57	<b>29.13</b>
	20	959	81	MO	TO	TO	3129.32	<b>TO</b>	MO	<b>26936</b>	TO	MO	<b>18.64</b>
	36	264	11	MO	0.77	TO	0.22	<b>0.51</b>	0.26	<b>0.37</b>	TO	MO	<b>1311.51</b>
	36	483	21	MO	21.41	TO	4.85	<b>8.31</b>	MO	<b>428.74</b>	TO	MO	<b>5069.82</b>
	49	364	11	MO	1.66	TO	0.45	<b>0.21</b>	0.75	<b>0.68</b>	TO	MO	<b>31203.92</b>

noisy quantum circuits. These baseline methods fall into three categories, each distinguished by its underlying data structure:

- **MM (Matrix Multiplication)-based methods:** MM-based methods represent quantum states, gates, and noise operators as matrices, with simulation performed via matrix multiplications. For this comparison, we adopt Qiskit’s `evolve` method as the representative MM-based approach.
- **DD (Decision Diagram)-based methods:** DD-based methods utilize tensor-like data structures to encode quantum states, gates, and noise operators. We evaluate two DD-based approaches: (1) the QMDD-based noise-aware simulator DDSIM [26], which adapts the stochastic quantum trajectory method from [26] for noisy circuit simulation, and (2) the Tensor Decision Diagram (TDD)-based method [47], modified from [34]. Additionally, we include the TDD-based equivalence checking tool from [34].
- **TN (Tensor Network)-based methods:** Tensor network-based methods are elaborated in Sections III, IV, and V. Here, ‘TN’ refers to the implementation of Algorithm 1, while ‘Ours’ denotes the approximate algorithms introduced in Sections IV and V. For comparison, we also implement a basic MPO-based method [28] using the same backend as our proposed methods.

### B. Experimental Comparison with Baseline Tools:

We compare our simulator with baseline simulators, presenting the results in Tables I and II. All methods are initially evaluated using a depolarizing noise model with  $\#Noise = 2$ , a noise type supported by all simulators, and a timeout

threshold of 3,600 seconds. For our method, we employ a level-1 approximation; the DDSIM simulator uses 30,000 samples. The noise-aware DDSIM simulator supports circuits up to 100 qubits; unsupported circuits are denoted by ‘-’. As shown in Table I, tensor network (TN)-based methods (TN and ours) outperform matrix multiplication (MM)- and decision diagram (DD)-based methods across most benchmark circuits, including QFT, VQE, QAOA, and Supremacy. Given that our approximation algorithm extends the TN-based approach, their efficiencies are comparable at this low noise level. These findings indicate that TN-based methods are more effective for simulating quantum circuits with practical applications, such as quantum machine learning (VQE and QAOA).

Next, we focus on comparing our method with TN-based simulators under higher noise numbers, where TN-based methods struggle. To demonstrate this, we increase the noise instances to 20, adopt a decoherence noise model, and extend the timeout threshold to 36,000 seconds to accommodate the increased computational demand. The results, reported in the  $\#Noise = 20$  columns of TABLE I, show that while the TN-based method often fails for circuits with larger noise levels, our approximation algorithm maintains strong performance. We also assess equivalence checking, comparing our method with TDD and TN. These findings confirm that our approximation algorithm surpasses the TN-based method in efficiency for circuits with a larger number of noises.

Additionally, we compare our approximation method with the MPO-based method, with results detailed in TABLE II for complex quantum circuits. The precision and runtime of the MPO-based method depend on its bond dimension, which we tuned to match the runtime of our algorithm. According to TABLE II, our method achieves higher precision than

the MPO-based approach under similar execution times. This indicates that our approximation algorithm offers a superior trade-off between efficiency and precision compared to the MPO-based method.

### C. Comparison with the Quantum Trajectories Method:

Our method is not limited to TN-based simulation. By employing singular value decomposition (SVD) to express noise operators as matrices, we decompose the computational tasks of noisy simulation and equivalence checking into multiple subtasks. These subtasks can be executed using various techniques, allowing our method—akin to the quantum trajectories approach—to offer a versatile approximation scheme compatible with diverse backends. In this section, we compare our approximation scheme with the quantum trajectories method, emphasizing efficiency and precision.

The runtime of the quantum trajectories method depends on the error bound and the probability that the result falls within this bound [16, 26]. To ensure a fair comparison, we set the success probability of the quantum trajectories method to 99%. Using Hoeffding’s inequality, achieving an accuracy of  $\delta$  with a probability exceeding 99% requires the quantum trajectories method to use  $\frac{\ln(100)}{2\delta^2}$  samples, whereas our method, at approximation level 1, needs only  $6n + 2$  samples, where  $n$  is the noise number. We evaluated the sample requirements for the quantum trajectories method to match the error bound of our algorithm at approximation level 1 across different noise rates  $p$ . For  $p = 0.001$  and  $p = 0.0001$ , with  $n$  ranging from 10 to 40, our method surpasses the quantum trajectories method when  $n \leq 26$  at  $p = 0.001$ , and consistently for all  $n$  at  $p = 0.0001$  (see Fig. 7). This analysis extends to both simulation and equivalence checking tasks.

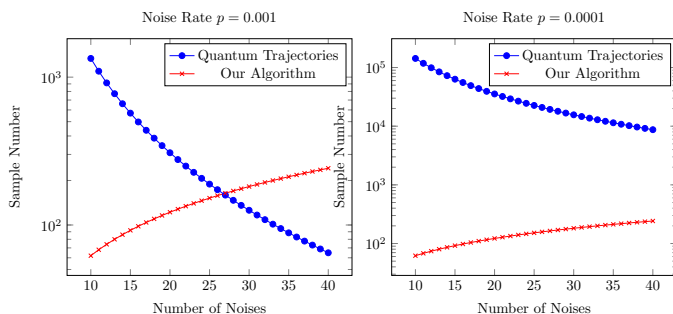


Fig. 7: Comparison of sample number required for the same error bound

Furthermore, we performed numerical experiments to compare the efficiency and precision of our method with the quantum trajectories method, with results presented in Table III. The quantum trajectories method was implemented in two variants: an MM-based simulator [16] and a TN-based simulator. Using a TN backend for the quantum trajectories method ensures a fair comparison by aligning the underlying framework with our approach. Both experiments employed a depolarizing noise model with a noise number of 20 and a noise rate of  $p = 0.001$ . We tuned the sample size of the quantum trajectories method to achieve the same precision

as our level-1 approximation. As shown in Table III, our method outperforms the quantum trajectories method (denoted “Traj”) in efficiency at equivalent precision levels. Notably, our algorithm surpasses the TN-based quantum trajectories method, despite sharing the same backend, highlighting the superior efficiency of our underlying scheme.

### D. Results on Noise

1) *Results on Noise Number:* Furthermore, to highlight the high efficiency of our approximation algorithm with respect to the number of noise instances, we simulate and check the equivalence of the 100-qubit QAOA circuit with 0 to 80 noise instances, as shown in Fig. 8. Our approximation algorithm handles all cases, while the TN-based method runs out of memory once the number of noise instances reaches 30. The primary reason for this memory failure is that increasing the number of noise instances can increase the maximum rank of the nodes in the tensor network contraction, leading to higher time and memory consumption during contraction. In comparison, when using the level-1 approximation of Algorithm 2, the runtime of our approximation algorithm increases almost linearly with the number of noise instances, as shown in Fig. 8, which is consistent with Theorem. 1.

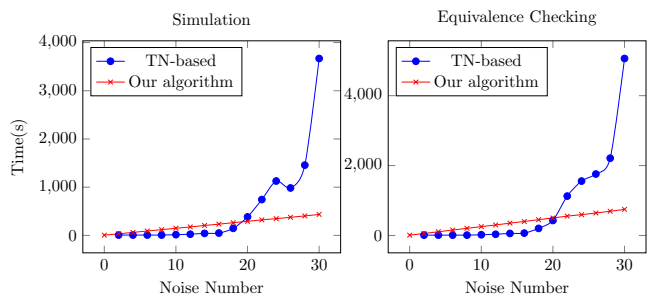


Fig. 8: The number of noise and runtime

2) *Results on Noise Rate:* The accuracy of our simulation and equivalence checking algorithm depends on the noise rate of the noises, i.e.,  $p = \|M_{\mathcal{E}_D} - I\|$ . When  $p$  is small, the algorithms has a high accuracy. We evaluated our algorithms under both the realistic model and the depolarizing noise model. In both cases, the results as shown in Fig. 9a and 9b demonstrate that as the noise rate increases, the approximation error also rises. It confirms that our approximation algorithm has better accuracy for lower noise rates in realistic noise models, which indicates a promising outlook for achieving higher precision on advanced hardware implementations in the future.

3) *Results on Approximation Levels:* Our algorithms offers varying levels of approximation, presenting a trade-off between computational efficiency and accuracy. As a demonstration, we simulate and check equivalence of the 64-qubit QAOA circuit with 10 noises. In simulation task the input state  $|\psi\rangle = |0\rangle \otimes \dots \otimes |0\rangle$  and  $|v\rangle = U|0\rangle \otimes \dots \otimes |0\rangle$ , where  $U$  represents the unitary operator of the ideal circuit. Table. IV shows the result for the same circuit with approximation levels from 0 to 3. From the result, we can see that the accuracy is

TABLE II: OUR ALGORITHM V.S. MPO-BASED METHODS

Type	Qubits	Gates	Depth	Simulation				Equivalence Checking					
				Bond	Time		Precision		Bond	Time		Precision	
					MPO	Ours	MPO	Ours		MPO	Ours		
QAOA	121	3322	42	400	803.38	<b>408.05</b>	8.94E-05	<b>1.28E-05</b>	800	1501.85	<b>2709.46</b>	7.59E-05	<b>1.06E-05</b>
	169	4706	42	400	2604.05	<b>2749.51</b>	2.89E-05	<b>4.82E-05</b>	600	4761.68	<b>4897.58</b>	2.41E-05	<b>5.38E-05</b>
	196	5488	42	400	3392.5	<b>4839.57</b>	1.47E-04	<b>1.49E-05</b>	600	6406.01	<b>8496.4</b>	1.02E-05	<b>1.27E-05</b>
Supermacy	16	115	11	200	18.91	<b>12.84</b>	1.30E-02	<b>2.87E-04</b>	400	34.17	<b>6.23</b>	1.29E-03	<b>3.16E-04</b>
	16	209	21	200	36.59	<b>28.88</b>	9.00E-03	<b>3.29E-04</b>	400	69.08	<b>9.03</b>	7.32E-04	<b>3.25E-04</b>
	16	299	31	200	58.85	<b>49.61</b>	2.30E-02	<b>7.39E-04</b>	400	108.89	<b>30.85</b>	2.29E-03	<b>7.63E-04</b>
	16	394	41	200	77.32	<b>68.18</b>	3.80E-02	<b>2.94E-04</b>	400	143.60	<b>78.4</b>	3.34E-03	<b>3.58E-04</b>
	20	145	11	400	103.57	<b>14.47</b>	2.94E-02	<b>4.52E-04</b>	600	189.71	<b>29.13</b>	2.63E-03	<b>4.43E-04</b>
	20	261	21	400	233.03	<b>69.82</b>	1.13E-02	<b>7.28E-04</b>	600	421.62	<b>18.64</b>	1.01E-03	<b>6.32E-04</b>
	20	378	31	400	309.93	<b>289.49</b>	6.80E-02	<b>3.51E-04</b>	800	1583.43	<b>1311.51</b>	6.62E-03	<b>4.37E-04</b>
36	264	11	300	389.47	<b>329.88</b>	3.83E-03	<b>1.84E-04</b>	1200	5707.40	<b>5069.82</b>	3.07E-04	<b>2.09E-04</b>	

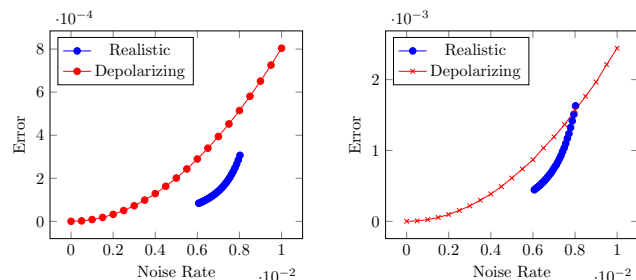
TABLE III: OUR ALGORITHM V.S. APPROXIMATE METHODS

Circuit	Precision			Runtime		
	Ours	Traj (MM)	Traj (TN)	Ours	Traj (MM)	Traj (TN)
QAOA_6	<b>1.55E-04</b>	1.43E-04	1.80E-04	<b>4.56</b>	1.49	10.84
QAOA_10	<b>5.96E-05</b>	1.98E-04	2.00E-04	<b>7.57</b>	10.94	19.68
QAOA_15	<b>9.03E-05</b>	2.55E-04	2.66E-04	<b>8.41</b>	658.38	25.48
QAOA_64	<b>5.82E-07</b>	MO	3.48E-07	<b>191.47</b>	MO	598.62
QAOA_100	<b>1.03E-07</b>	MO	1.30E-07	<b>361.79</b>	MO	1264.67

TABLE IV: ACCURACY FOR DIFFERENT APPROXIMATION LEVELS

Level	Simulation		Equivalence Checking	
	Time (s)	Error	Time (s)	Error
0	0.34	4.59E-03	1.74	1.33E-02
1	11.18	3.02E-05	39.48	8.86E-05
2	109.95	1.23E-06	183.96	3.60E-06
3	1971.37	1.13E-06	3029.5	3.28E-06

getting higher as expected, but the cost for an extra level of approximation is also significant. For most scenarios, the level-1 approximation is recommended since it can achieve a good balance between runtime and accuracy.



(a) Simulation error

(b) Equivalence checking error

Fig. 9: Error at different noise rate

## VII. CONCLUSION

In this paper, we introduced approximation algorithms for simulating and checking the equivalence of noisy quantum circuits. By representing noisy quantum circuits with tensor network diagrams and utilizing singular value decomposition (SVD) for approximation, our algorithm outperforms existing methods in terms of speed, while maintaining the same approximation accuracy. The algorithm is implemented using Google’s TensorNetwork for tensor contraction. We demonstrate the utility and effectiveness of our approach through experiments on noisy simulation and equivalence checking, using various benchmark circuits with realistic noise models. The results show that our algorithm can efficiently simulate and check the equivalence of a QAOA circuit with approximately 200 qubits and 20 noise channels.

Future research could improve noise handling. Our algorithm manages 20 channels for larger-scale real-application NISQ circuits, but real NISQ circuits have noise per gate and other multiple qubit noise (e.g., crosstalk), requiring scalable solutions. Optimizing tensor contraction for circuit topologies (e.g., QAOA, VQE) could also cut computational costs beyond current heuristics. Practically, our approach could enhance quantum SDKs (e.g., Qiskit, Cirq) for circuit optimization, benchmark hardware, and prototype large-scale models for quantum machine learning and optimization. Given its scalability, we expect our algorithm to be integrated into current ATPG programs (e.g., [48, 49, 50, 41]) for verifying and detecting manufacturing defects in large-scale quantum circuits affected by quantum noise.

## ACKNOWLEDGMENTS

This work was partly supported by the Youth Innovation Promotion Association, Chinese Academy of Sciences (Grant No. 2023116) and the National Natural Science Foundation of China (Grant No. 62402485).

## REFERENCES

- [1] F. Arute, K. Arya, R. Babbush, D. Bacon, J. C. Bardin, R. Barends, R. Biswas, S. Boixo, F. G. Brandao, D. A. Buell *et al.*, “Quantum supremacy using a programmable superconducting processor,” *Nature*, vol. 574, no. 7779, pp. 505–510, 2019.
- [2] G. Q. AI *et al.*, “Quantum error correction below the surface code threshold,” *Nature*, vol. 638, no. 8052, p. 920, 2024.
- [3] J. Gambetta, “The hardware and software for the era of quantum utility is here,” 2023.
- [4] J. Preskill, “Quantum computing in the NISQ era and beyond,” *Quantum*, vol. 2, p. 79, 2018.
- [5] P. W. Shor, “Scheme for reducing decoherence in quantum computer memory,” *Physical review A*, vol. 52, no. 4, p. R2493, 1995.
- [6] A. M. Steane, “Error correcting codes in quantum theory,” *Physical Review Letters*, vol. 77, no. 5, p. 793, 1996.
- [7] Y. Ueno, M. Kondo, M. Tanaka, Y. Suzuki, and Y. Tabuchi, “QECCOL: On-line quantum error correction with a superconducting decoder for surface code,” in *2021 58th ACM/IEEE Design Automation Conference (DAC)*. IEEE, 2021, pp. 451–456.
- [8] K. Temme, S. Bravyi, and J. M. Gambetta, “Error mitigation for short-depth quantum circuits,” *Physical review letters*, vol. 119, no. 18, p. 180509, 2017.
- [9] S. Endo, S. C. Benjamin, and Y. Li, “Practical quantum error mitigation for near-future applications,” *Physical Review X*, vol. 8, no. 3, p. 031027, 2018.
- [10] H. Zhang, L. Lu, S. Tan, S. Zheng, J. Yu, and J. Yin, “SpREM: Exploiting hamming sparsity for fast quantum readout error mitigation,” in *Proceedings of the 61st ACM/IEEE Design Automation Conference*, 2024, pp. 1–6.
- [11] M. Harrigan, K. J. Sung, K. Satzinger, M. Neeley, F. C. Arute, K. Arya, J. Atalaya, J. Bardin, R. Barends, S. Boixo, M. B. Broughton, B. B. Buckley, D. A. Buell, B. Burkett, N. Bushnell, J. Chen, Y. Chen, B. Chiaro, R. Collins, W. Courtney, S. Demura, A. Dunsworth, A. Fowler, B. R. Foxen, C. M. Gidney, M. Giustina, R. Graff, S. Habegger, S. Hong, L. Ioffe, S. Isakov, E. Jeffrey, Z. Jiang, C. Jones, D. Kafri, K. Kechedzhi, J. Kelly, S. Kim, P. Klimov, A. Korotkov, F. Kostritsa, D. Landhuis, P. Laptev, M. Leib, M. Lindmark, O. Martin, J. Martinis, J. R. McClean, M. McEwen, A. Megrant, X. Mi, M. Mohseni, W. Mruczkiewicz, J. Mutus, O. Naaman, C. Neill, F. Neukart, M. Y. Niu, T. E. O’Brien, B. O’Gorman, A. Petukhov, H. Putterman, C. Quintana, P. Roushan, N. Rubin, D. Sank, A. Skolik, V. Smelyanskiy, D. Strain, M. Streif, M. Szalay, A. Vainsencher, T. White, J. Yao, A. Zalcman, L. Zhou, H. Neven, D. Bacon, E. Lucero, E. Farhi, and R. Babbush, “Quantum approximate optimization of non-planar graph problems on a planar superconducting processor,” *Nature Physics*, 2021. [Online]. Available: <https://www.nature.com/articles/s41567-020-01105-y>
- [12] Google AI Quantum and Collaborators, F. Arute, K. Arya, R. Babbush, D. Bacon, J. C. Bardin, R. Barends, S. Boixo, M. Broughton, B. B. Buckley, D. A. Buell, B. Burkett, N. Bushnell, Y. Chen, Z. Chen, B. Chiaro, R. Collins, W. Courtney, S. Demura, A. Dunsworth, E. Farhi, A. Fowler, B. Foxen, C. Gidney, M. Giustina, R. Graff, S. Habegger, M. P. Harrigan, A. Ho, S. Hong, T. Huang, W. J. Huggins, L. Ioffe, S. V. Isakov, E. Jeffrey, Z. Jiang, C. Jones, D. Kafri, K. Kechedzhi, J. Kelly, S. Kim, P. V. Klimov, A. Korotkov, F. Kostritsa, D. Landhuis, P. Laptev, M. Lindmark, E. Lucero, O. Martin, J. M. Martinis, J. R. McClean, M. McEwen, A. Megrant, X. Mi, M. Mohseni, W. Mruczkiewicz, J. Mutus, O. Naaman, M. Neeley, C. Neill, H. Neven, M. Y. Niu, T. E. O’Brien, E. Ostby, A. Petukhov, H. Putterman, C. Quintana, P. Roushan, N. C. Rubin, D. Sank, K. J. Satzinger, V. Smelyanskiy, D. Strain, K. J. Sung, M. Szalay, T. Y. Takeshita, A. Vainsencher, T. White, N. Wiebe, Z. J. Yao, P. Yeh, and A. Zalcman, “Hartree-fock on a superconducting qubit quantum computer,” *Science*, vol. 369, no. 6507, pp. 1084–1089, 2020. [Online]. Available: <https://www.science.org/doi/abs/10.1126/science.abb9811>
- [13] S. Boixo, S. Isakov, V. Smelyanskiy, R. Babbush, N. Ding, Z. Jiang, M. J. Bremner, J. Martinis, and H. Neven, “Characterizing quantum supremacy in near-term devices,” *Nature Physics*, vol. 14, p. 595–600, 2018. [Online]. Available: <https://www.nature.com/articles/s41567-018-0124-x>
- [14] L.-T. Wang, C.-W. Wu, and X. Wen, *VLSI test principles and architectures: design for testability*. Elsevier, 2006.
- [15] C. Roberts, A. Milsted, M. Ganahl, A. Zalcman, B. Fontaine, Y. Zou, J. Hidary, G. Vidal, and S. Leichenauer, “Tensornetwork: A library for physics and machine learning,” 2019.
- [16] S. V. Isakov, D. Kafri, O. Martin, C. V. Heidweiller, W. Mruczkiewicz, M. P. Harrigan, N. C. Rubin, R. Thomson, M. Broughton, K. Kissell *et al.*, “Simulations of quantum circuits with approximate noise using qsim and cirq,” *arXiv preprint arXiv:2111.02396*, 2021.
- [17] T. Häner and D. S. Steiger, “5 petabyte simulation of a 45-qubit quantum circuit,” in *Proceedings of the International Conference for High Performance Computing, Networking, Storage and Analysis*, 2017, pp. 1–10.
- [18] C. Huang, F. Zhang, M. Newman, J. Cai, X. Gao, Z. Tian, J. Wu, H. Xu, H. Yu, B. Yuan *et al.*, “Classical simulation of quantum supremacy circuits,” *arXiv preprint arXiv:2005.06787*, 2020.
- [19] R. Li, B. Wu, M. Ying, X. Sun, and G. Yang, “Quantum supremacy circuit simulation on sunway taihulight,” *IEEE Transactions on Parallel and Distributed Systems*, vol. 31, no. 4, pp. 805–816, 2019.
- [20] E. Pednault, J. A. Gunnels, G. Nannicini, L. Horesh, T. Magerlein, E. Solomonik, and R. Wisnieff, “Breaking the 49-qubit barrier in the simulation of quantum circuits,” *arXiv preprint arXiv:1710.05867*, vol. 15, 2017.
- [21] B. Villalonga, S. Boixo, B. Nelson, C. Henze, E. Rieffel, R. Biswas, and S. Mandrà, “A flexible high-performance simulator for verifying and benchmarking quantum cir-

- cuits implemented on real hardware,” *npj Quantum Information*, vol. 5, no. 1, pp. 1–16, 2019.
- [22] F. Pan and P. Zhang, “Simulation of quantum circuits using the big-batch tensor network method,” *Phys. Rev. Lett.*, vol. 128, p. 030501, 1 2022. [Online]. Available: <https://link.aps.org/doi/10.1103/PhysRevLett.128.030501>
- [23] Y.-H. Tsai, J.-H. R. Jiang, and C.-S. Jhang, “Bit-slicing the hilbert space: Scaling up accurate quantum circuit simulation,” in *2021 58th ACM/IEEE Design Automation Conference (DAC)*. IEEE Press, 2021, p. 439–444. [Online]. Available: <https://doi.org/10.1109/DAC18074.2021.9586191>
- [24] A. Zulehner and R. Wille, “Advanced simulation of quantum computations,” *IEEE Transactions on Computer-Aided Design of Integrated Circuits and Systems*, vol. 38, no. 5, pp. 848–859, 2018.
- [25] S. Hillmich, R. Kueng, I. L. Markov, and R. Wille, “As accurate as needed, as efficient as possible: Approximations in dd-based quantum circuit simulation,” in *2021 Design, Automation & Test in Europe Conference & Exhibition (DATE)*. IEEE, 2021, pp. 188–193.
- [26] T. Grurl, J. Fuß, and R. Wille, “Noise-aware quantum circuit simulation with decision diagrams,” *IEEE Transactions on Computer-Aided Design of Integrated Circuits and Systems*, pp. 1–1, 2022.
- [27] Y. Zhou, E. M. Stoudenmire, and X. Waintal, “What limits the simulation of quantum computers?” *Physical Review X*, vol. 10, no. 4, p. 041038, 2020.
- [28] K. Woolfe, “Matrix product operator simulations of quantum algorithms,” Ph.D. dissertation, University of Melbourne, School of Physics, 2015.
- [29] K. Noh, L. Jiang, and B. Fefferman, “Efficient classical simulation of noisy random quantum circuits in one dimension,” *Quantum*, vol. 4, p. 318, 2020.
- [30] S. Cheng, C. Cao, C. Zhang, Y. Liu, S.-Y. Hou, P. Xu, and B. Zeng, “Simulating noisy quantum circuits with matrix product density operators,” *Physical Review Research*, vol. 3, no. 2, p. 023005, 2021.
- [31] P. Niemann, R. Wille, and R. Drechsler, “Equivalence checking in multi-level quantum systems,” in *Reversible Computation: 6th International Conference, RC 2014, Kyoto, Japan, July 10-11, 2014. Proceedings 6*. Springer, 2014, pp. 201–215.
- [32] L. Burgholzer and R. Wille, “Advanced equivalence checking for quantum circuits,” *IEEE Transactions on Computer-Aided Design of Integrated Circuits and Systems*, vol. 40, no. 9, pp. 1810–1824, 2020.
- [33] —, “Improved dd-based equivalence checking of quantum circuits,” in *2020 25th Asia and South Pacific Design Automation Conference (ASP-DAC)*. IEEE, 2020, pp. 127–132.
- [34] X. Hong, M. Ying, Y. Feng, X. Zhou, and S. Li, “Approximate equivalence checking of noisy quantum circuits,” in *2021 58th ACM/IEEE Design Automation Conference (DAC)*, 2021, pp. 637–642.
- [35] X. Hong, Y. Feng, S. Li, and M. Ying, “Equivalence checking of dynamic quantum circuits,” in *Proceedings of the 41st IEEE/ACM International Conference on Computer-Aided Design*, 2022, pp. 1–8.
- [36] M. Huang, J. Guan, W. Fang, and M. Ying, “Approximation algorithm for noisy quantum circuit simulation,” in *2024 Design, Automation & Test in Europe Conference & Exhibition (DATE)*. IEEE, 2024, pp. 1–6.
- [37] M. A. Nielsen and I. L. Chuang, *Quantum computation and quantum information*. Cambridge university press, 2010.
- [38] Q. Huang, B. Li, M. Gao, and M. Ying, “Fault models in superconducting quantum circuits,” 2022. [Online]. Available: <https://arxiv.org/abs/2212.00337>
- [39] J. Biamonte and V. Bergholm, “Tensor networks in a nutshell,” *arXiv preprint arXiv:1708.00006*, 2017.
- [40] I. L. Markov and Y. Shi, “Simulating quantum computation by contracting tensor networks,” *SIAM Journal on Computing*, vol. 38, no. 3, pp. 963–981, 2008.
- [41] K. Chen and M. Ying, “Automatic test pattern generation for robust quantum circuit testing,” *ACM Transactions on Design Automation of Electronic Systems*, vol. 29, no. 6, pp. 1–36, 2024.
- [42] J. Watrous, *The theory of quantum information*. Cambridge university press, 2018.
- [43] C. Eckart and G. Young, “The approximation of one matrix by another of lower rank,” *Psychometrika*, vol. 1, no. 3, pp. 211–218, 1936.
- [44] A. Gilchrist, N. K. Langford, and M. A. Nielsen, “Distance measures to compare real and ideal quantum processes,” *Physical Review A—Atomic, Molecular, and Optical Physics*, vol. 71, no. 6, p. 062310, 2005.
- [45] K. Chen, W. Fang, J. Guan, X. Hong, M. Huang, J. Liu, Q. Wang, and M. Ying, “Veriqbench: A benchmark for multiple types of quantum circuits,” *arXiv preprint arXiv:2206.10880*, 2022.
- [46] Quantum AI team and collaborators, “Recirq,” Oct. 2020. [Online]. Available: <https://doi.org/10.5281/zenodo.4091470>
- [47] X. Hong, X. Zhou, S. Li, Y. Feng, and M. Ying, “A tensor network based decision diagram for representation of quantum circuits,” *ACM Trans. Des. Autom. Electron. Syst.*, vol. 27, no. 6, 6 2022. [Online]. Available: <https://doi.org/10.1145/3514355>
- [48] X. Fang-ying, C. Han-wu, L. Wen-jie, and L. Zhi-giang, “Fault detection for single and multiple missing-gate faults in reversible circuits,” in *2008 IEEE Congress on Evolutionary Computation (IEEE World Congress on Computational Intelligence)*. IEEE, 2008, pp. 131–135.
- [49] A. Paler, I. Polian, and J. P. Hayes, “Detection and diagnosis of faulty quantum circuits,” in *17th Asia and South Pacific Design Automation Conference*. IEEE, 2012, pp. 181–186.
- [50] D. Bera, “Detection and diagnosis of single faults in quantum circuits,” *IEEE Transactions on Computer-Aided Design of Integrated Circuits and Systems*, vol. 37, no. 3, pp. 587–600, 2017.